## References


1. Vogelzang NJ, Rusthoven JJ, Symanowski J, Denham C, Kaukel E, Ruffie P, Gatzemeier U, Boyer M, Emri S, Manegold C, Niyikiza C, Paoletti P. Phase III study of pemetrexed in combination with cisplatin versus cisplatin alone in patients with malignant pleural mesothelioma. *J Clin Oncol* 2003;21:2636–44.
2. Pelucchi C, Malvezzi M, La Vecchia C, Levi F, Decarli A, Negri E. The Mesothelioma epidemic in Western Europe: an update. *Br J Cancer* 2004;90: 1022–4.
3. Leigh J, Driscoll T. Malignant mesothelioma in Australia, 1945–2002. *Int J Occup Environ Health* 2003;9:206–17.
4. Leithner K, Leithner A, Clar H, Weinhaeusel A, Radl R, Krippl P, Rehak P, Windhager R, Haas OA, Olschewski H. Mesothelioma mortality in Europe: impact of asbestos consumption and simian virus 40. *Orphanet J Rare Dis* 2006;1:44.
5. Murayama T, Takahashi K, Natori Y, Kurumatani N. Estimation of future mortality from pleural malignant mesothelioma in Japan based on an age-cohort model. *Am J Ind Med* 2006;49:1–7.
6. Fitzpatrick DR, Peroni DJ, Bielefeldt-Ohmann H. The role of growth factors and cytokines in the tumorigenesis and immunobiology of malignant mesothelioma. *Am J Respir Cell Mol Biol* 1995;12:455–60.
7. Galffy G, Mohammed KA, Dowling PA, Nasreen N, Ward MJ, Antony VB. Interleukin 8: an autocrine growth factor for malignant mesothelioma. *Cancer Res* 1999;59:367–71.
8. Lee TC, Zhang Y, Aston C, Hintz R, Jagirdar J, Perle MA, Burt M, Rom WN. Normal human mesothelial cells and mesothelioma cell lines express insulin-like growth factor I and associated molecules. *Cancer Res* 1993;53:2858–64.
9. Morocz IA, Schmitter D, Lauber B, Stahel RA. Autocrine stimulation of a human lung mesothelioma cell line is mediated through the transforming growth factor alpha/epidermal growth factor receptor mitogenic pathway. *Br J Cancer* 1994;70: 850–6.
10. Versnel MA, Claesson-Welsh L, Hanmacher A, Bouts MJ, van der Kwast TH, Eriksson A, Willemsen R, Weima SM, Hoogsteden HC, Hagemeijer A, et al. Human malignant mesothelioma cell lines express PDGF beta-receptors whereas cultured normal mesothelial cells express predominantly PDGF alpha-receptors. *Oncogene* 1991;6:2005–11.
11. Monti G, Jaurand MC, Monnet I, Chretien P, Saint-Etienne L, Zeng L, Portier A, Devillier P, Galanaud P, Bignon J, et al. Intrapleural production of interleukin 6 during mesothelioma and its modulation by gamma-interferon treatment. *Cancer Res* 1994;54:4419–23.
12. Adachi Y, Aoki C, Yoshio-Hoshino N, Takayama K, Curiel DT, Nishimoto N. Interleukin-6 induces both cell growth and VEGF production in malignant mesotheliomas. *Int J Cancer* 2006;119: 1303–11.
13. Buettner R, Mora LB, Jove R. Activated STAT signaling in human tumors provides novel molecular targets for therapeutic intervention. *Clin Cancer Res* 2002;8: 945–54.
14. Endo TA, Masuhara M, Yokouchi M, Suzuki R, Sakamoto H, Mitsui K, Matsumoto A, Tanimura S, Ohtsubo M, Misawa H, Miyazaki T, Leonor N, et al. A new protein containing an SH2 domain that inhibits JAK kinases. *Nature* 1997;387: 921–4.
15. Naka T, Narazaki M, Hirata M, Matsumoto T, Minamoto S, Aono A, Nishimoto N, Kajita T, Taga T, Yoshizaki K, Akira S, Kishimoto T. Structure and function of a new STAT-induced STAT inhibitor. *Nature* 1997;387:924–9.
16. Starr R, Willson TA, Viney EM, Murray LJ, Rayner JR, Jenkins BJ, Gonda TJ, Alexander WS, Metcalf D, Nicola NA, Hilton DJ. A family of cytokine-inducible inhibitors of signalling. *Nature* 1997;387: 917–21.
17. Rakesh K, Agrawal DK. Controlling cytokine signaling by constitutive inhibitors. *Biochem Pharmacol* 2005;70: 649–57.
18. Naka T, Fujimoto M, Tsutsui H, Yoshimura A. Negative regulation of cytokine and TLR signalings by SOCS and others. *Adv Immunol* 2005;87:61–122.
19. Yoshimura A, Naka T, Kubo M. SOCS proteins, cytokine signalling and immune regulation. *Nat Rev Immunol* 2007;7: 454–65.
20. Nicholson SE, De Souza D, Fabri LJ, Corbin J, Willson TA, Zhang JG, Silva A, Asimakis M, Farley A, Nash AD, Metcalf D, Hilton DJ, et al. Suppressor of cytokine signaling-3 preferentially binds to the SHP-2-binding site on the shared cytokine receptor subunit gp130. *Proc Natl Acad Sci USA* 2000;97:6493–8.
21. He B, You L, Uematsu K, Zang K, Xu Z, Lee AY, Costello JF, McCormick F, Jablons DM. SOCS-3 is frequently silenced by hypermethylation and suppresses cell growth in human lung cancer. *Proc Natl Acad Sci USA* 2003;100: 14133–8.
22. Bromberg J. Stat proteins and oncogenesis. *J Clin Invest* 2002;109:1139–42.
23. Sekido Y. Genomic abnormalities and signal transduction dysregulation in malignant mesothelioma cells. *Cancer Sci* 2010;101:1–6.
24. Poulikakos PI, Xiao GH, Gallagher R, Jablonski S, Jhanwar SC, Testa JR. Re-expression of the tumor suppressor NF2/merlin inhibits invasiveness in mesothelioma cells and negatively regulates FAK. *Oncogene* 2006;25: 5960–8.
25. Lehmann U, Schmitz J, Weissenbach M, Sobota RM, Hortner M, Friederichs K, Behrmann I, Tsiaris W, Sasaki A, Schneider-Mergener J, Yoshimura A, Neel BG, et al. SHP2 and SOCS3 contribute to Tyr-759-dependent attenuation of interleukin-6 signaling through gp130. *J Biol Chem* 2003;278:661–71.
26. Liu E, Cote JF, Vuori K. Negative regulation of FAK signaling by SOCS proteins. *EMBO J* 2003;22:5036–46.
27. Niwa Y, Kanda H, Shikauchi Y, Saiura A, Matsubara K, Kitagawa T, Yamamoto J, Kubo T, Yoshikawa H. Methylation silencing of SOCS-3 promotes cell growth and migration by enhancing JAK/STAT and FAK signalings in human hepatocellular carcinoma. *Oncogene* 2005; 24:6406–17.
28. Miyake S, Makimura M, Kanegae Y, Harada S, Sato Y, Takamori K, Tokuda C, Saito I. Efficient generation of recombinant adenoviruses using adenovirus DNA-terminal protein complex and a cosmid bearing the full-length virus genome. *Proc Natl Acad Sci USA* 1996;93: 1320–4.
29. Kijima T, Osaki T, Nishino K, Kumagai T, Funakoshi T, Goto H, Tachibana I, Tanio Y, Kishimoto T. Application of the Cre recombinase/loxP system further enhances antitumor effects in cell type-specific gene therapy against carcinoembryonic antigen-producing cancer. *Cancer Res* 1999;59: 4906–11.
30. Goto H, Osaki T, Kijima T, Nishino K, Kumagai T, Funakoshi T, Kimura H, Takeda Y, Yoneda T, Tachibana I, Hayashi S. Gene therapy utilizing the Cre/loxP system selectively suppresses tumor growth of disseminated carcinoembryonic antigen-producing cancer cells. *Int J Cancer* 2001; 94:414–9.
31. Nishino K, Osaki T, Kumagai T, Kijima T, Tachibana I, Goto H, Arai T, Kimura H, Funakoshi T, Takeda Y, Tanio Y, Hayashi S. Adenovirus-mediated gene therapy specific for small cell lung cancer cells using a Myc-Max binding motif. *Int J Cancer* 2001;91:851–6.
32. Kanegae Y, Makimura M, Saito I. A simple and efficient method for purification of

infectious recombinant adenovirus. *Jpn J Med Sci Biol* 1994;47:157–66.

33. Lipka DB, Hoffmann LS, Heidel F, Markova B, Blum MC, Breitenbuecher F, Kasper S, Kindler T, Levine RL, Huber C, Fischer T. LS104, a non-ATP-competitive small-molecule inhibitor of JAK2, is potently inducing apoptosis in JAK2V617F-positive cells. *Mol Cancer Ther* 2008;7:1176–84.
34. Verstovsek S, Manshouri T, Quintas-Cardama A, Harris D, Cortes J, Giles FJ, Kantarjian H, Priebe W, Estrov Z. WP1066, a novel JAK2 inhibitor, suppresses proliferation and induces apoptosis in erythroid human cells carrying the JAK2 V617F mutation. *Clin Cancer Res* 2008;14:788–96.
35. Vazquez A, Bond EE, Levine AJ, Bond GL. The genetics of the p53 pathway, apoptosis and cancer therapy. *Nat Rev Drug Discov* 2008;7:979–87.
36. Yonesaka K, Tamura K, Kurata T, Satoh T, Ikeda M, Fukuoka M, Nakagawa K. Small interfering RNA targeting survivin sensitizes lung cancer cell with mutant p53 to adriamycin. *Int J Cancer* 2006;118: 812–20.
37. Sakaguchi K, Sakamoto H, Lewis MS, Anderson CW, Erickson JW, Appella E, Xie D. Phosphorylation of serine 392 stabilizes the tetramer formation of tumor suppressor protein p53. *Biochemistry* 1997; 36:10117–24.
38. Hao M, Lowy AM, Kapoor M, Deffie A, Liu G, Lozano G. Mutation of phosphoserine 389 affects p53 function in vivo. *J Biol Chem* 1996;271:29380–5.
39. D'Orazi G, Cecchinelli B, Bruno T, Manni I, Higashimoto Y, Saito S, Gostissa M, Coen S, Marchetti A, Del Sal G, Piaggio G, Fanciulli M, et al. Homeodomain-interacting protein kinase-2 phosphorylates p53 at Ser 46 and mediates apoptosis. *Nat Cell Biol* 2002;4:11–9.
40. Saito S, Goodarzi AA, Higashimoto Y, Noda Y, Lees-Miller SP, Appella E, Anderson CW. ATM mediates phosphorylation at multiple p53 sites, including Ser(46), in response to ionizing radiation. *J Biol Chem* 2002; 277:12491–4.
41. Abbas T, Dutta A. p21 in cancer: intricate networks and multiple activities. *Nat Rev Cancer* 2009;9:400–14.
42. Calabrese V, Mallette FA, Deschenes-Simard X, Ramanathan S, Gagnon J, Moores A, Ilangumaran S, Ferbeyre G. SOCS1 links cytokine signaling to p53 and senescence. *Mol Cell* 2009;36:754–67.
43. Sterman DH, Recio A, Carroll RG, Gillespie CT, Haas A, Vachani A, Kapoor V, Sun J, Hodinka R, Brown JL, Corbley MJ, Parr M, et al. A phase I clinical trial of single-dose intrapleural IFN-beta gene transfer for malignant pleural mesothelioma and metastatic pleural effusions: high rate of antitumor immune responses. *Clin Cancer Res* 2007;13: 4456–66.
44. Sterman DH, Recio A, Vachani A, Sun J, Cheung L, DeLong P, Amin KM, Litzky LA, Wilson JM, Kaiser LR, Albelda SM. Long-term follow-up of patients with malignant pleural mesothelioma receiving high-dose adenovirus herpes simplex thymidine kinase/ganciclovir suicide gene therapy. *Clin Cancer Res* 2005;11:7444–53.

Fujii et al. Radiation Oncology 2011, 6:8
http://www.ro-journal.com/content/6/1/8

RADIATION ONCOLOGY

RESEARCH Open Access

# Cationized gelatin-HVJ envelope with sodium borocaptate improved the BNCT efficacy for liver tumors *in vivo*

Hitoshi Fujii[1], Akifumi Matsuyama[2], Hiroshi Komoda[1], Masao Sasai[2], Minoru Suzuki[3], Tomoyuki Asano[4], Yuichiro Doki[1], Mitsunori Kirihata[4], Koji Ono[3], Yasuhiko Tabata[5], Yasufumi Kaneda[6], Yoshiki Sawa[1], Chun Man Lee[1,2,7*]

**Abstract**

**Background:** Boron neutron capture therapy (BNCT) is a cell-selective radiation therapy that uses the alpha particles and lithium nuclei produced by the boron neutron capture reaction. BNCT is a relatively safe tool for treating multiple or diffuse malignant tumors with little injury to normal tissue. The success or failure of BNCT depends upon the $^{10}B$ compound accumulation within tumor cells and the proximity of the tumor cells to the body surface. To extend the therapeutic use of BNCT from surface tumors to visceral tumors will require $^{10}B$ compounds that accumulate strongly in tumor cells without significant accumulation in normal cells, and an appropriate delivery method for deeper tissues.
Hemagglutinating Virus of Japan Envelope (HVJ-E) is used as a vehicle for gene delivery because of its high ability to fuse with cells. However, its strong hemagglutination activity makes HVJ-E unsuitable for systemic administration. In this study, we developed a novel vector for $^{10}B$ (sodium borocaptate: BSH) delivery using HVJ-E and cationized gelatin for treating multiple liver tumors with BNCT without severe adverse events.

**Methods:** We developed cationized gelatin conjugate HVJ-E combined with BSH (CG-HVJ-E-BSH), and evaluated its characteristics (toxicity, affinity for tumor cells, accumulation and retention in tumor cells, boron-carrying capacity to multiple liver tumors *in vivo*, and bio-distribution) and effectiveness in BNCT therapy in a murine model of multiple liver tumors.

**Results:** CG-HVJ-E reduced hemagglutination activity by half and was significantly less toxic in mice than HVJ-E. Higher $^{10}B$ concentrations in murine osteosarcoma cells (LM8G5) were achieved with CG-HVJ-E-BSH than with BSH. When administered into mice bearing multiple LM8G5 liver tumors, the tumor/normal liver ratios of CG-HVJ-E-BSH were significantly higher than those of BSH for the first 48 hours ($p < 0.05$). In suppressing the spread of tumor cells in mice, BNCT treatment was as effective with CG-HVJ-E-BSH as with BSH containing a 35-fold higher $^{10}B$ dose. Furthermore, CG-HVJ-E-BSH significantly increased the survival time of tumor-bearing mice compared to BSH at a comparable dosage of $^{10}B$.

**Conclusion:** CG-HVJ-E-BSH is a promising strategy for the BNCT treatment of visceral tumors without severe adverse events to surrounding normal tissues.

* Correspondence: tg4c_1211@help.med.osaka-u.ac.jp
[1]Department of Surgery, Osaka University Graduate School of Medicine, Osaka, Japan
Full list of author information is available at the end of the article

## Background

Boron neutron capture therapy (BNCT) is a cell-selective radiation therapy that uses alpha particles and lithium nuclei produced by the boron neutron capture reaction. These particles cause cell destruction, bouncing out to a maximum distance of 10 μm from the target, a distance that corresponds to the size of a cell. These particles only destroy the cells that take up $^{10}$Boron ($^{10}$B) [1]. This therapy is clinically indicated for multiple and diffuse tumors, such as glioblastoma and head and neck tumors [2]. BNCT was recently evaluated for treating liver tumors [3-8], although the prognosis of patients treated by BNCT with conventional $^{10}$B compounds, particularly sodium borocaptate (BSH), is not good because of its low accumulation in liver tumors and the attenuation of the epithermal neutron beams directed toward deep lesions [9-11]. Therefore, treating liver tumors effectively with BNCT will require novel ways of delivering BSH, with the characteristics of high accumulation in the tumor, low toxicity for normal tissue, and rapid withdrawal from normal tissue and the bloodstream [12]. Various carriers such as liposomes have been investigated [13-16], but until now a vector for BSH that adequately satisfies the above requirements has not been developed.

Liver tumors, including primary and secondary tumors, are the fifth most common solid tumor worldwide. The incidence is increasing rapidly in most countries, at a pace that will make liver tumors the third most common tumor by 2030 [17,18]. The mortality rate of liver tumors, especially multiple metastatic liver tumors, is high. Multimodal therapies for multiple liver tumors have advanced considerably, and include radiofrequency ablation, radiation, surgical extirpation and transplantation [19]. However, therapy for multiple and diffuse liver tumors is still difficult, because reducing the liver volume reduces its organ function. Therefore, a therapy selective for tumors with minimal damage to normal liver tissue is of great interest.

Hemagglutinating Virus of Japan Envelope (HVJ-E) is a simple vector that is converted into an inactivated virus containing lipid envelope for gene transfer vector originally [20]. HVJ-E has been used to carry anticancer drugs with some success [21,22]. HVJ-E is reported both to possess high fusion ability and to elicit anti-tumor immune responses [23,24], making it an attractive candidate for widespread use in cancer therapy. On the other hand, HVJ-E has strong hemagglutination activity, making it unsuitable to administer systemically. There are no reports describing the systemic administration of HVJ-E in cancer therapy, although one study reports improved HVJ-E stability in the bloodstream when it is administered with a cationized gelatin [25]. The development of a novel HVJ-E-based vector that can be administered into the general circulation is highly desirable for cancer treatment.

We therefore focused on HVJ-E because of its versatility, its high fusion ability, and its ability to stimulate an immune response. We developed a cationized gelatin conjugate of HVJ-E with BSH that can be administered into the general circulation, and we evaluated its safety, bio-distribution, and effectiveness in BNCT treatment using a murine model of multiple liver tumors.

## Materials and methods

### Mice

Female C3H/HeN Jcl mice at 8-12 weeks of age were obtained from CLEA Japan (Tokyo, Japan) and kept in standard housing. Body weight of mice was 19.6 ± 1.6 (17-23) g at each experiment. All animal experiments were performed under a protocol approved by the Ethics Review Committee for Animal Experimentation of Osaka University Graduate School of Medicine.

### Cell line

The cell line of murine osteosarcoma (LM8G5), which was isolated from LM8 cells after five successive cycles of *in vivo* selection procedures, were used because of their high potential for metastasizing to the liver [26,27]. The cells were maintained in D-MEM (Sigma Aldrich Japan, Tokyo, Japan) containing 10% fetal bovine serum, 1% (v/v) 100 × non-essential amino acids, 1 mM sodium pyruvate, 2 mM L-glutamine, 50 μM 2-mercaptoethanol, 100 units/ml penicillin, and 100 μg/ml streptomycin.

### Animal Model

LM8G5 cells ($1 \times 10^6$ cells in 200 μl, with serum-free medium) were injected into the surgically exposed ileocolic vein of mice under general anesthesia with Avertin (2.5% tribromoethanol at a concentration of 1 ml/100 g live weight). Multiple small liver tumors were observed seven days after the injection by exploratory laparotomy, and these tumors led to the death of the mice within 20 days after tumor inoculation.

### HVJ-E

HVJ was purified from chicken egg chorioallantoic fluid by centrifugation, and the titer calculated as previously described [20]. The virus was inactivated by UV irradiation exposure (99 mJ/cm$^2$) just before use, eliminating the ability of the virus to replicate while leaving its fusion capacity intact, as previously described [20].

### Cationized Gelatin (CG) and BSH

Gelatin was prepared from pig skin type I collagen through an acid process, and was kindly supplied by Nitta Gelatin (Osaka, Japan). Ethylenediamine (ED),

glutaraldehyde, 2,4,6-trinitrobenzenesulfonic acid, β-alanine, and a protein assay kit (# L8900) were purchased from Nacalai Tesque (Kyoto, Japan). The coupling agent, 1-ethyl-3-(3-dimethylaminopropyl) carbodiimide hydrochloride salt (EDC), was obtained from Dojindo Laboratories (Kumamoto, Japan). The CG was prepared by introducing ED to the carboxyl groups of low-molecular-weight gelatin (M.W. 3,100), as previously described [28]. Sodium borocaptate ($Na_2\ ^{10}B_{12}H_{11}SH$: BSH), was obtained from Stella Chemifa (Osaka, Japan).

### Incorporation into HVJ-E

To incorporate plasmid DNA or BSH into HVJ-E, 10 μl of HVJ-E suspension ($1.0 \times 10^{10}$ particles) was added to 15 μl of 1% protamine sulfate, and this was mixed with plasmid DNA (200 μg) or BSH (6,667 μg boron) and 40 μl of 3% Tween-80 diluted with TE solution (10 mM Tris-HCl, pH 8.0, 1 mM EDTA). Qdot 655 ITK Carboxyl Quantum Dots (Qdot; Invitrogen, Carlsbad, CA, USA) were introduced into HVJ-E by electroporation (250 V, 750 μF). The mixture was centrifuged at 15,000 rpm for 15 min at 4°C. To remove the detergent and unincorporated plasmid DNA, BSH, or Qdot, the pellet was washed with 1 ml of balanced salt solution (10 mM Tris-HCl, pH 7.5, 137 mM NaCl, and 5.4 mM KCl), and the envelope vector was suspended in 1,000 μl of phosphate-buffered saline (PBS). To determine the $^{10}B$ concentration in the HVJ-E combined with BSH, the complex was digested with nitric acid solution at Bio Research (Hyogo, Japan) and assayed with inductively coupled plasma-atomic emission spectrometry (ICP-AES, ULTIMA2, Horiba Jobin Yvon, Kyoto, Japan).

### Cationized Gelatin conjugate HVJ-E (CG-HVJ-E)

The CG-HVJ-E complex was formed by mixing the two materials in an aqueous solution. Briefly, 750 μg of CG was added to 150 μl of 0.1 M PBS (pH 7.4) containing $4.5 \times 10^9$ particles of HVJ-E. The solution was mixed by tapping several times. The solution was then incubated on ice for 15 min to form CG-HVJ-E. The CG-HVJ-E vector was purified by centrifugation as described above.

### Zeta potential and particle size of HVJ-E compounds

The zeta potential of each HVJ-E complex (HVJ-E, CG-HVJ-E, HVJ-E-BSH, and CG-HVJ-E-BSH) was measured by an electrophoretic light scattering (ELS) assay (ELS-7000AS, Otsuka Electric Co. Ltd., Osaka, Japan) at 37°C with an electric field strength of 100 V/cm [29]. The particle size of each compound was measured by a dynamic light scattering (DLS) assay (Submicron Particle Analyzer N5, Beckman Coulter, Fullerton, CA, USA).

### Transmission microscopy

Ultra-thin layers of HVJ-E, CG-HVJ-E, and CG-HVJ-E-BSH stained with 3% uranylacetate were examined with an electron microscope (H-7650 and S-800, Hitachi, Tokyo, Japan) to determine the particle size.

### Hemagglutination assay

The hemagglutination assay was done in a 96-well round-bottom plate using 50 μl/well of a 0.5% suspension of chicken red blood cells (Nippon Bio-Test Laboratories, Tokyo, Japan) and 50 μl/well of an HVJ-E solution serially diluted with PBS [30].

### Acute toxicity in normal mice

Each HVJ-E complex was administered by intra-cardiac injection (200 μl) into 8-12-week-old female C3H/HeN mice, which were monitored for 7 days for survival.

### Blood chemistry monitoring after systemic administration of HVJ-E complexes

Indications of systemic injury were recorded, including serum levels of total bilirubin (T. Bil), aspartate aminotransferase (AST), and alanine aminotransferase (ALT) as markers of liver function, lactate dehydrogenase (LDH) and blood urea nitrogen (BUN) as markers of hemagglutination, and creatinine (Cr) as a marker of renal function. All marker levels were measured using an automated analyzing system (BML, Tokyo, Japan) at 24 and 48 hours and at 7 days after systemic administration of $4.5 \times 10^9$ HVJ-E particles.

### Affinity of HVJ-E complexes to tumor cells and localization of Qdot carried in HVJ-E complexes

HVJ-E ($1.5 \times 10^9$ particles) and CG (250 μg) were combined to produce CG-HVJ-E. LM8G5 cells ($2 \times 10^4$) were seeded into each well of an 8-well Lab-tek chamber (Nalge Nunc International, Rochester, NY, USA) and cultured overnight. The cells were incubated with Qdot alone or Qdot with HVJ-E or CG-HVJ-E, at a concentration of $2.5 \times 10^8$ Qdot particles per well for 1 hour. The cells were washed twice with PBS and fixed with 4% paraformaldehyde. Hoechst 33342 (10 μM, Invitrogen) was used to stain the nuclei, and the cells were viewed with fluorescence microscopy (BX61, Olympus, Tokyo, Japan). To visualize the intracellular localization of the Qdot carried in the HVJ-E or CG-HVJ-E, the cells were stained with Hoechst 33342 for the nucleus and Alexa Fluor 488 phalloidin (Invitrogen) for the cytoplasm, and were viewed by confocal microscopy (Fluoview FV1000, Olympus).

### Transfection efficiency of HVJ-E complexes into tumor cells

The various HVJ-E complexes were incubated with tumor cells to evaluate their transfection efficiency. LM8G5 cells ($2 \times 10^4$) were seeded into each well of a 96-well plate, cultured overnight with 200 μl of culture medium, and washed with PBS. Each HVJ-E complex

with or without luciferase-expressing plasmids (50 μl; $1.5 \times 10^9$ particles) was incubated with tumor cells for 30 min, and then incubated for 30 min at 37°C. After washing twice with PBS, the cells were incubated with fresh medium for 24 hours and then lysed with Lysis Buffer (Promega, Madison, WI, USA). Luciferase activity in the cells was then measured with a Luciferase Assay kit (Promega) using a fluorescence plate reader (Mithras LB 940, Berthold Technologies, Bad Wildbad, Germany). The protein content of the samples was assayed by the Bradford method [31].

#### Accumulation and retention of BSH or CG-HVJ-E-BSH in tumor cells *in vitro*

Tumor cells of the LM8G5 cell line ($1 \times 10^6$) were seeded in 75 $cm^2$ tissue culture flasks and were cultured overnight. The cells were then washed with PBS, 1 ml of BSH (20 μg boron/ml) or CG-HVJ-E-BSH (20 μg boron/ml) was added to each flask, and the mixture was incubated for 30 min at 37°C. The cells were then washed twice with PBS, and the $^{10}B$ concentration in the cells was immediately measured by ICP-AES (Horiba Jobin Yvon) as the initial $^{10}B$ value bound to the cells. Other flasks were incubated an additional 24-48 hours at 37°C and the cells were double-washed again before being tested for $^{10}B$ concentration, which was measured as the $^{10}B$ value.

#### Bio-distribution of BSH or CG-HVJ-E-BSH in normal or liver tumor-bearing mice

Mice were injected with 200 μl of BSH (35 μg boron/g ) or 200 μl of CG-HVJ-E-BSH (1.2 μg boron/g ), administered into the general circulation. At 1, 24, or 48 hours after the injection, mice were sacrificed and peripheral blood samples collected. The lung, liver, kidney and spleen were removed after whole-body perfusion with heparinized saline, and weighted. The extracted tissues were digested with the M-Per mammalian protein extraction reagent (Pierce Chemical Co., Rockford, IL, USA) and ultrasonic homogenizer (H3-350, Kawajiri Machinery, Hyogo, Japan), and the $^{10}B$ concentration in each sample was measured by ICP-AES (Horiba Jobin Yvon). The $^{10}B$ accumulation into each organ was calculated as the percentage of $^{10}B$ per weight of each organ.

#### Neutron capture autoradiography imaging of murine liver sections after BSH or CG-HVJ-E-BSH administration

Mice bearing liver tumors were given either 35 μg boron/g of BSH or 1.2 μg boron/g of CG-HVJ-E-BSH, administered into the general circulation. The mice were sacrificed 1 hour after BSH administration or 24 hours after CG-HVJ-E-BSH administration. The liver was removed after whole-body perfusion with heparinized saline. Frozen 16-μm-thick liver sections were mounted on Baryotrak-P detector plates (Nagase-Landauer, Tokyo, Japan) and air-dried for 60 min. The samples were exposed to thermal neutrons at a rate of $2.1 \times 10^{13}$ neutrons/$m^2 \cdot s^1$ for 1 hour at the Japan Research Reactor 4 (JRR-4). For α-auto-radiographic imaging, the detector plates were etched in 7 N NaOH at 70°C for 2 hours to reveal the proton tracks produced by the boron neutron capture reaction [32]. The number of α particles per 10,000 $\mu m^2$ in each section was counted using VH Analyzer software (Biozero, Keyence, Osaka, Japan).

#### Antitumor efficacy of BNCT for murine liver tumors with BSH or CG-HVJ-E-BSH

Mice bearing liver tumors were irradiated with a thermal neutron beam at the JRR-4 8 days after tumor cell inoculation. The mice were given 1.2 μg boron/g of CG-HVJ-E-BSH 24 hours before irradiation treatment, or 35 μg boron/g of BSH 1 hour before irradiation treatment, administered into the general circulation. The mice were then set the acrylic stand, and irradiated for 17 min at the Japan Research Reactor 4 (JRR-4). Neutron irradiation was performed in a single fraction using an thermal beam mode I of JRR-4. In the in-air beam characteristics, thermal neutron flux and the γ-ray absorbed dose were $2.1 \times 10^{13}$ neutrons/$m^2 \cdot s^1$ and 3.6 Sv/h at a reactor power of 3.5 MW, respectively. To evaluate the effect of BNCT treatment on the liver tumors, the mice were sacrificed 6 days after irradiation, and the livers removed, weighed, and evaluated for pathologic changes. In a separate experiment, 1.2 μg boron/g of BSH or 1.3 μg boron/g of CG-HVJ-E-BSH was administered, the mice were either irradiated or not, and their survival time after irradiation was recorded.

#### Statistical analyses

Student's *t*-test was used to determine whether the differences between the various groups were significant. Differences between groups in the survival experiment were determined using the Kaplan-Meier log-rank test. A *p*-value of less than 0.05 was considered statistically significant.

## Results

#### CG-HVJ-E characteristics

SDS-PAGE results confirmed that when mixed and centrifuged with HVJ-E, the CG bound to HVJ-E in a dose-dependent manner within a certain range (data not shown). The optimal ratio of CG to HVJ-E, in which the CG-HVJ-E containing luciferase plasmid was transferred most efficiently into LM8G5 cells (data not shown), was identified as 1 μg to $6.0 \times 10^6$ particles, and the zeta potential and particle size of the resulting CG-HVJ-E conjugate was measured (Table 1). CG- HVJ-E was

**Table 1 Zeta potential and particle sizes of each HVJ-E complex**

| Complex | Apparent molecular size (nm) | Zeta potential (mV) |
|---|---|---|
| HVJ-E | 293 ± 32 | -25 ± 1 |
| CG-HVJ-E | 297 ± 21 | -15 ± 3 |
| HVJ-E-BSH | 448 ± 144 | -28 ± 1 |
| CG-HVJ-E-BSH | 494 ± 196 | -19 ± 2 |

more positive (-14.7 mV) than HVJ-E (-25.1 mV). The form and size of these particles were estimated by using Transmission Electron Microscopy (TEM) and Scanning Electron Microscopy (SEM). HVJ-E, CG-HVJ-E, and CG-HVJ-E-BSH were approximately 300, 300, and 500 nm in diameter, respectively, as measured by TEM (Additional file 1, Figure S1). The DLS assay results were similar (data not shown). Therefore, these data are able to give an estimate that incorporating BSH into the HVJ-E complexes made them larger and slightly more positive than either HVJ-E or CG-HVJ-E.

### CG-HVJ-E had less hemagglutination activity in vitro and was less toxic than HVJ-E in mice

Hemagglutination is caused by hemagglutinin-neuramidase (HN) protein on the HVJ-E membrane [33]. The hemagglutination of chicken blood cells by CG-HVJ-E was approximately half that of HVJ-E (data not shown). The acute toxicity was determined by administering various concentrations of HVJ-E or CG-HVJ-E to normal mice and monitoring their survival over 7 days; the 100% survival dosage of CG-HVJ-E ($6.0 \times 10^9$ particles) was higher than that of HVJ-E ($4.5 \times 10^9$ particles). Blood tests done 24 hours after the administration of $4.5 \times 10^9$ particles of HVJ-E or $4.5 \times 10^9$ particles of CG-HVJ-E showed that blood chemistry markers in the CG-HVJ-E-treated mice were almost within the normal range, while those in the HVJ-E-treated mice were significantly higher (Figure 1). These levels peaked 24 hours after administration in mice treated with HVJ-E, and became normal at 7 days (data not shown).

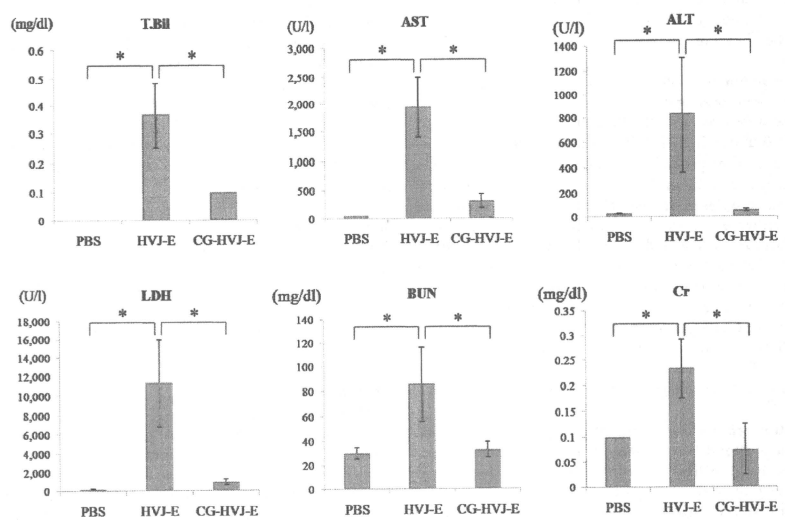


**Figure 1 Blood chemistry tests 24 hours after HVJ-E and CG-HVJ-E administration into normal mice.** Blood markers (T.Bil, AST, ALT, LDH, BUN, and Cr) in normal mice tested 24 hours after intra-cardiac injection of PBS, HVJ-E or CG-HVJ-E. * $p < 0.05$. Results shown are the means ± SD ($n = 4$).

### High affinity and infusion ability of CG-HVJ-E in tumor cells

CG-HVJ-E containing Qdot had a higher affinity for tumor cells than Qdot alone or HVJ-E containing Qdot (Figure 2A). CG-HVJ-E containing Qdot was taken into the cytoplasm, and some Qdots were localized to the nuclei, as seen by confocal microscopy (Figure 2B).

### CG-HVJ-E transfection into tumor cells *in vitro* was highly efficient

CG-HVJ-E's *in vitro* transfection efficiency into tumor cells was 4 times greater than that of HVJ-E, as assessed by a luciferase assay, and it was not cytotoxic (Figure 2C). The enhanced transfection efficiency of CG-HVJ-E was also observed in another tumor cell line (CT26: murine colon cancer, data not shown).

### CG-HVJ-E-BSH increased $^{10}B$ accumulation and retention in tumor cells *in vitro* compared to BSH

The concentration of $^{10}B$ was significantly higher in cells incubated with CG-HVJ-E-BSH than in those incubated with BSH ($p < 0.05$). The $^{10}B$ levels gradually decreased in both cell groups, but the levels were significantly higher in the cells incubated with CG-HVJ-E-BSH than

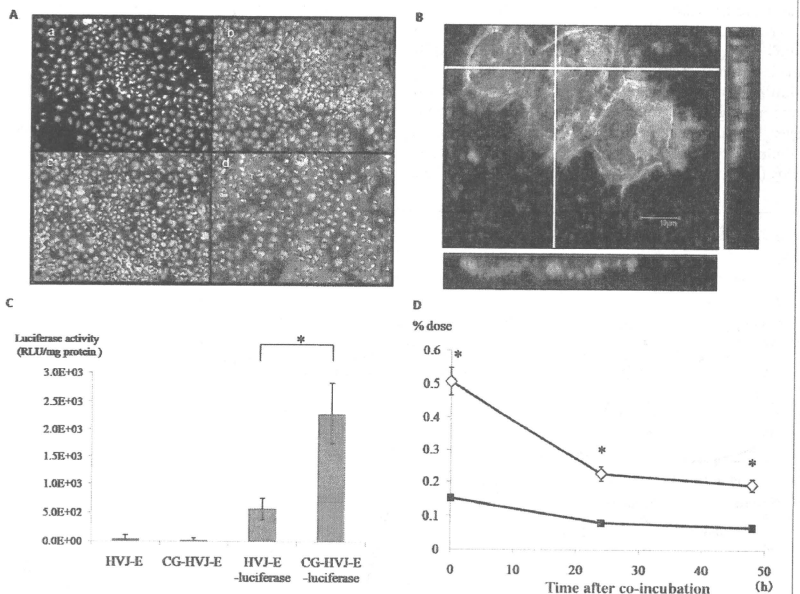


**Figure 2 Affinity of CG-HVJ-E for tumor cells and the intracellular uptake of molecules incorporated into HVJ-E.** A) Affinity of HVJ-E and CG-HVJ-E for tumor cells. LM8G5 cells were incubated alone (a), or with Qdot (b), HVJ-E-Qdot (c), or CG-HVJ-E-Qdot (d) for 60 min in a Lab-tek chamber slide and examined for Qdot (red) and Hoechst 33342 (blue) by fluorescence microscopy. Representative views are shown. B) Intracellular localization of Qdot transported by CG-HVJ-E. Tumor cells were incubated with CG-HVJ-E-Qdot (orange) and stained with Hoechst 33342 (blue) and Alexa Fluor 488 phalloidin (green). Image shows 3-dimensional analysis with confocal microscopy. C) Luciferase activity in tumor cells transfected with HVJ-E or CG-HVJ-E. Cells were cultured for 30 min with HVJ-E or CG-HVJ-E containing a luciferase-expressing plasmid. Luciferase activity was measured 24 hours later to evaluate the transfection efficiency. Results are shown as means ± SD (n = 4). Similar results were obtained in three experiments. * $p < 0.05$. D) $^{10}B$ accumulation and retention in tumor cells *in vitro*. Cells were incubated with 20 μg boron/ml of BSH or CG-HVJ-E-BSH for 30 min, then washed twice with PBS, and the $^{10}B$ concentration was measured by ICP-AES. Separately, cells were incubated in the same manner, but after washing, were incubated in medium without BSH for 24 or 48 hours before testing for $^{10}B$ concentration as described above. The horizontal axis shows time after co-incubation. The vertical axis shows the percent of the administered dose (% dose) of CG-HVJ-E-BSH (open diamond) or BSH (solid square). Results shown are the means ± S.D. (n = 3). * $p < 0.05$.

in those with BSH for at least 48 hours after incubation (Figure 2D). These results indicate that CG-HVJ-E-BSH binds rapidly to tumor cells and that the $^{10}B$ contained in CG-HVJ-E-BSH is internalized into the cytoplasm or the nucleus. Adding CG-HVJ-E-BSH to tumor cells *in vitro* resulted in sufficient $^{10}B$ accumulation and retention in the cells to be useful for BNCT.

### BSH incorporated into CG-HVJ-E accumulated in liver tumors and rapidly disappeared from normal tissues in tumor-bearing mice

In normal mice, the $^{10}B$ concentration in the liver 1 hour after administration was higher with BSH than with CG-HVJ-E-BSH. The concentration of both compounds started to decrease by 48 hours after administration. The $^{10}B$ concentration in the lung, kidney, and spleen was low at all time points with both compounds (Figure 3A). In the liver tumor model, BSH and CG-HVJ-E-BSH behaved similarly in the normal liver tissue surrounding the tumors (Figure 3B, middle panel). In the tumors, however, the concentration of $^{10}B$ at 1 and 24 hours after administration was significantly higher with CG-HVJ-E-BSH (34.76 and 10.71% dose/g) than with BSH (2.21 and 2.29% dose/g) (Figure 3B, left panel). In the bloodstream, the $^{10}B$ concentration at 1 hour after administration tended to be higher with CG-HVJ-E-BSH (20.9% dose/ml) than with BSH (7.96% dose/ml), despite the lower quantity of $^{10}B$ administered with both boron compounds (1.2 μg boron/g). From 24 hours after administration and onward, the concentration of $^{10}B$ from both compounds was the same (Figure 3B, right panel).

### Tumor/Normal liver $^{10}B$ ratio in murine liver tumors was greater with CG-HVJ-E-BSH

The Tumor/Normal (T/N) liver $^{10}B$ ratio with CG-HVJ-E-BSH was significantly higher than with BSH from 1 to 48 hours after administration ($p < 0.05$), with a peak difference at 24 hours ($p < 0.05$; Figure 3C). The Tumor/Blood $^{10}B$ ratio of CG-HVJ-E-BSH also remained higher than that of BSH from 1 to 48 hours after administration (data not shown).

### CG-HVJ-E-BSH improved the T/N $^{10}B$ ratio in neutron capture autoradiography images of murine liver tumors

Neutron capture autoradiography (NCAR) was performed after BSH (35 μg boron/g) or CG-HVJ-E-BSH

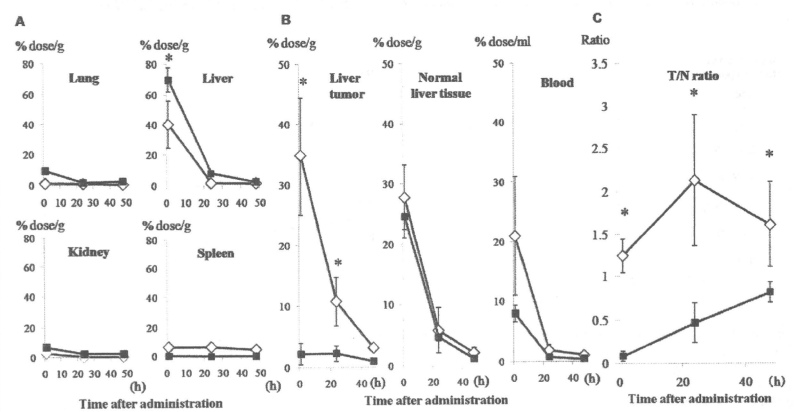


**Figure 3 Bio-distribution of $^{10}B$ in mice with normal liver or with liver tumors.** A) Time course of organ (lung, liver, kidney, and spleen) uptake of $^{10}B$ delivered by 1.2 μg boron/g of BSH or CG-HVJ-E-BSH in normal mice. B) Time course of tumor accumulation (left panel), liver uptake (middle panel), and blood residence (right panel) of $^{10}B$ delivered by 1.2 μg boron/g of BSH or CG-HVJ-E-BSH in tumor-bearing mice. The horizontal axis shows the time after administration. The vertical axis shows the percent of the administered dose per gram of tissue (% dose/g). C) Time course of the Tumor-to-Normal liver tissue (T/N) $^{10}B$ concentration ratio for CG-HVJ-E-BSH (open diamond) or BSH solution (solid square). Data are expressed as the mean ± S.D. ($n = 3$). * $p < 0.05$ compared with BSH.

(1.2 μg boron/g) was injected into mice bearing liver tumors. The $^{10}B$ particle count in the BSH- and CG-HVJ-E-BSH-treated livers are shown in Figure 4B and 4C. The T/N ratio 1 hour after BSH administration was 0.12, and that for CG-HVJ-E-BSH at 24 hours after administration was 2.76 (Figure 4D), which is similar to the values obtained in the bio-distribution study. It is of interest that the T/N $^{10}B$ ratio was higher with CG-HVJ-E-BSH, even though the actual quantity of $^{10}B$ was 30 times greater in the BSH dosage. The number of α particles with CG-HVJ-E (415 ± 35) was similar to that of BSH (451 ± 107) in the liver tumor sections (Figure 4A).

### BNCT with CG-HVJ-E-BSH inhibited tumor growth, preserved the normal surrounding liver tissue, and prolonged survival time in the murine liver tumor model

To evaluate the use of BNCT with CG-HVJ-E-BSH for murine liver tumors, BNCT was performed on mice bearing LM8G5 liver tumors. To assess the T/N ratio of CG-HVJ-E-BSH, BNCT was performed 24 hours after CG-HVJ-E-BSH administration or 1 hour after BSH administration [2,4]. We first evaluated the anti-tumor efficacy at 14 days after tumor cell inoculation, because up to that time, the tumor-bearing mice were severely damaged by the radical spread of tumors (about 50% of the untreated mice were dead). Therefore, we sacrificed the tumor-bearing mice that were alive until that time to evaluate the efficacy of BNCT.

BNCT with CG-HVJ-E-BSH (1.2 μg boron/g) inhibited the local growth of liver metastases as much as BNCT with BSH (35 μg boron/g). This dosage of BSH was determined from the clinical dose for BNCT for various malignant tumors, and effectively contained 35 times the $^{10}B$ that was present in the CG-HVJ-E-BSH dosage (Figure 5A, B). Some histological damage, which appeared, for example as fractionated or vacuolated

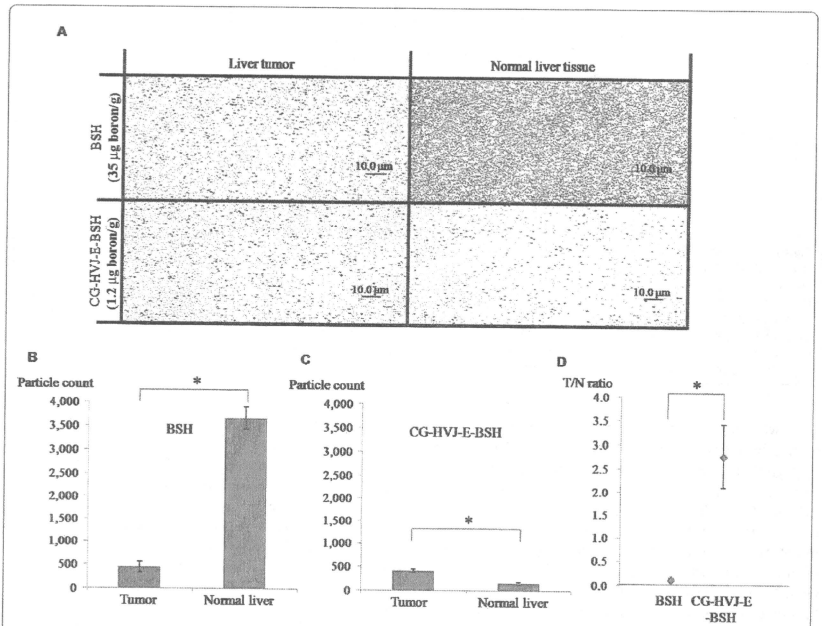


**Figure 4 Neutron capture radiographic image in murine liver sections after administration of BSH or CG-HVJ-E-BSH.** Liver sections from tumor-bearing mice were prepared and frozen 1 hour after BSH (35 μg boron/g) injection or 24 hours after CG-HVJ-E-BSH (1.2 μg boron/g) injection. The sections were placed on CR-39 detector plates and exposed to thermal neutrons ($2.1 \times 10^{13}$ neutrons/$m^2$·$s^1$) for 1 hour. A) The number of α particles per 10,000 $\mu m^2$ section was counted by VH Analyzer software after NaOH etching. B) The number of α particles per 10,000 $\mu m^2$ section of BSH or C) of CG-HVJ-E-BSH (n = 3). D) Tumor-to-normal liver tissue (T/N) ratio for the number of α particles.

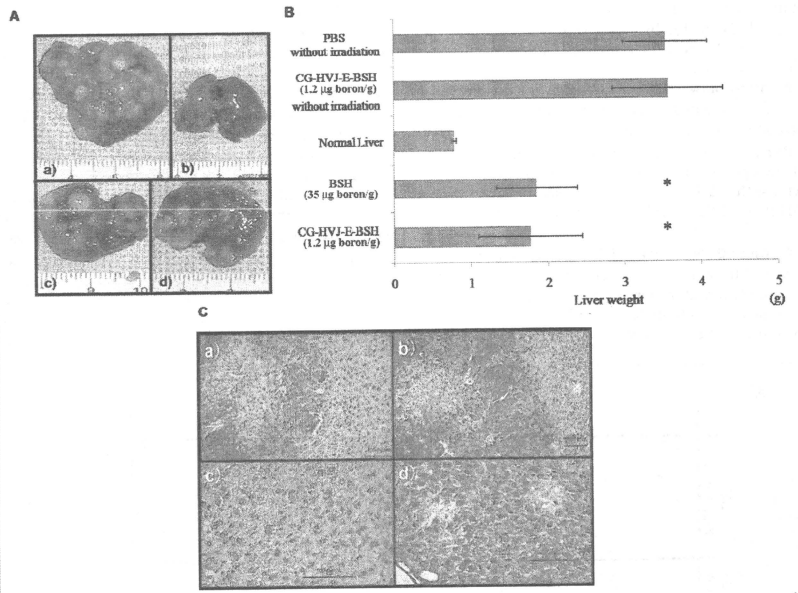


**Figure 5 Anti-tumor efficacy of BNCT in mice with liver tumors.** C3H/HeN mice were given an intra-portal injection of LM8G5 cells ($1 \times 10^6$ cells) on day 0. Mice were given a single intra-cardiac injection of CG-HVJ-E-BSH (1.2 μg boron/g) 24 hours before irradiation, or BSH (35 μg boron/g) 1 hour before irradiation. PBS and CG-HVJ-E-BSH solution were administered without neutron irradiation as a control. After irradiation on day 8, mice were sacrificed on day 14 to determine the BNCT efficacy on tumor metastasis. A) Macroscopic views (a) of the liver with tumors after administration of PBS; (b) normal liver; (c) liver with tumors after BNCT with BSH, and (d) liver with tumors after BNCT with CG-HVJ-E. B) Liver weight after BNCT. * $p < 0.05$ compared with PBS or CG-HVJ-E without irradiation. (each group n = 4). C) Representative light microscopic views of liver tumor tissue (upper panels, low magnification) or normal liver tissue (lower panels, high magnification) 6 days after BNCT with CG-HVJ-E-BSH (1.2 μg boron/g) (a, c) or BSH (35 μg boron/g) (b, d). Sections are stained with hematoxylin-eosin. Bar: 100 μm.

cells, was observed in both the tumor mass and in the normal liver tissue after BNCT with BSH (35 μg boron/g) (Figure 5C-b, d). In contrast, little histological damage was detected in the normal liver tissue surrounding the tumors after BNCT with CG-HVJ-E-BSH (Figure 5C-a, d). We originally thought that the damage to the liver might have been influenced by the longer survival time of mice treated with BSH and BNCT; however, the survival rate of these mice at 14 days after tumor cell inoculation was 37.5% (Additional file 2, Figure S2). This survival time was shorter than that of the untreated tumor-bearing mice. As we were not able to be certain if this dosage of BSH was a clinical equivalent, we used a dose of 1.3 μg boron/g of BSH to evaluate the survival time after BNCT, compared to a dose of 1.2 μg boron/g of CG-HVJ-E-BSH.

Finally, we compared the effectiveness of BNCT against tumors when used with BSH or CG-HVJ-E-BSH, in terms of survival after BNCT. With the assumption that the survival time of tumor-bearing mice after BNCT with a high dose of BSH (35 μg boron/g) was affected by normal liver damage as well as anti-tumor efficacy, both compounds were administered at dosages with similar $^{10}B$ concentrations (CG-HVJ-E-BSH, 1.2 μg boron/g or BSH,1.3 μg boron/g) into mice bearing liver tumors at 24 hours or 1 hour before irradiation, respectively. Irradiation was performed 8 days after the tumor cell inoculation, and the survival of the mice assessed.

CG-HVJ-E-BSH was most effective in increasing the mean survival time of mice bearing liver tumors compared with the other groups ($p < 0.005$; Additional file 2, Figure S2). We observed little histological damage in the normal liver tissues 6 days after BNCT with the lower dose of BSH (1.3 μg boron/g ) besides the damage that was already present in the tumor mass (Additional file 3, Figure S3).

## Discussion

With the goal of creating a novel BSH vector for effective BNCT, we chose HVJ-E because of its strong fusion ability, its effectiveness as a vehicle for delivering various drugs and genes, and its ability to stimulate an immune response against tumors in local cancer therapy [23]. Clinical trials of locally administered HVJ-E for patients with advanced malignant melanoma are underway in Japan. Although HVJ-E is not suitable for systemic administration because of its strong hemagglutinating activity, it has been reported that combining HVJ-E with 5,000-kDa cationized gelatin greatly improves its stability in the bloodstream [25]. In this study, we developed CG-HVJ-E combined with BSH, which can be administered into the general circulation, unlike HVJ-E, and confirmed its bio-distribution.

We compared the safety and efficacy of CG-HVJ-E-BSH in BNCT with that of BSH, using a murine model for liver tumors. For systemic administration, we developed a smaller CG-HVJ-E with a lower molecular weight (3,300 kDa) CG compared with the previously used CG-HVJ-E, which had a particle diameter of 777 nm [25]. We found that this CG-HVJ-E could be safely administered systemically in mice, with reduced toxicity and hemagglutination compared to HVJ-E (Figure 1). In the bio-distribution test using normal mice, both BSH and CG-HVJ-E-BSH accumulated in the liver immediately, but almost all of the $^{10}B$ had disappeared from the normal liver 48 hours later (Figure 3A). In liver tumors, however, CG-HVJ-E-BSH accumulation was greater than that of BSH although the boron proceeding from CG-HVJ-E-BSH was 35 times higher than that of BSH (Figure 3B); accordingly, the CG-HVJ-E-BSH T/N ratio was significantly higher than that of BSH in tumor-bearing mice, particularly at 24 hours after administration (Figure 3C). Neutron capture autoradiography revealed a higher T/N $^{10}B$ ratio with CG-HVJ-E-BSH than with BSH 1 hour after administration, despite the 35-fold-higher quantity of $^{10}B$ contained in the BSH dosage (Figure 4).

In our experiments, BNCT was performed 1 hour after BSH administration, because it followed the reported procedure for the clinical use of BNCT for liver tumors [9], and there was little difference between the T/N ratio an hour after administration and the ratio over the next 24 hours (Figure 3C). This was due to the protracted circulating time of CG-HVJ-E-BSH in the bloodstream. Therefore, this complex accumulated in the tumor by the enhanced permeability and retention (EPR) effect [34]. In fact, the particle size of the CG-HVJ-E-BSH was suitable for the EPR effect (Table 1) [35]. Another reason for this finding was that CG-HVJ-E has a high affinity and high fusion ability for tumor cells (Figure 2A, B, C). Although $^{10}B$ was taken up by the tumor cells over time, a large number of CG-HVJ-E-BSH molecules were incorporated into the tumor cells immediately, and high $^{10}B$ concentrations were maintained much longer with CG-HVJ-E-BSH than with BSH (Figure 2D). The mechanism for the preferential affinity of CG-HVJ-E to tumor cells as compared with HVJ-E has not been clarified, but it has been reported that when HVJ-E is conjugated with cationized gelatin, the transfection efficiency improves without a loss of cell fusion ability [25]. Therefore, the efficacy of CG-HVJ-E-BSH was similar to the 35-fold higher dose of $^{10}B$ as BSH for suppressing the spread of tumor cells without normal liver injury (Figure 5A, B, C).

When used in BNCT, the CG-HVJ-E-BSH significantly increased the survival time over BSH at an equivalent $^{10}B$ dosage (Additional file 2, Figure S2). Generally, BSH is rarely transferred into the cytoplasm and, once there, is easily removed [36]. On the other hand, CG-HVJ-E-BSH was highly selective for tumor cells and showed both strong fusion ability and the ability to transfer into the tumor cell nucleus. As a result, CG-HVJ-E-BSH improved the effectiveness of BNCT because the $^{10}B$ was highly concentrated and retained in the nuclei of the tumor cells (Figure 2B, C), where its cytotoxicity was much higher than that of $^{10}B$ bound to the tumor cell surface [14,37,38].

Moreover, HVJ-E has the potential to induce a bystander effect, so that CG-HVJ-E-BSH could be incorporated into vicinal cells through gap junctions. It is possible that BNCT with CG-HVJ-E-BSH induces a synergistic effect, resulting in a greater destruction of vicinal tumor cells than is seen with BNCT with BSH, which induces a bystander effect that generates hereditary abnormalities in vicinal cells [39].

We chose multiple liver tumors as a target for evaluating the effectiveness of BNCT with CG-HVJ-E-BSH, because BNCT for multiple liver tumors has not gained popularity and the T/N ratio needs to be improved for deep-site tumors. In the absence of liver function disorders, the response of multiple liver tumors is thought to be a good indication of BNCT effectiveness. In this report, we treated mice bearing liver tumors with BNCT [27] after establishing the presence of tumors of several millimeters in diameter. This murine model appears to reflect the clinical stage that we targeted. BNCT with BSH is not indicated for multiple liver tumors in clinical

settings and is only at the experimental stage [9,10]. BNCT was significantly more effective against liver tumors when used with CG-HVJ-E-BSH than with BSH, and normal liver tissue was not injured. The limited injury to normal liver tissue makes more than one BNCT irradiation possible, which is likely to increase the therapeutic potential. However, in these experiments, only one irradiation was done. With regard to BNCT with BSH for clinical liver tumors at deep sites, the required T/N $^{10}$B ratio is over 15 [36,40]. Moreover, the human trunk is much thicker than the murine trunk. Therefore, for BNCT with CG-HVJ-E-BSH to become an established, effective clinical procedure, further improvements are needed not only in the drug-delivery system, but also in the vessel-selective delivery [41] because of the attenuation of neutron beams directed toward deep lesions.

Our trial of BNCT for multiple liver tumors at deep sites should forward its development to treat other deep-site tumors, such as pancreatic cancer and malignant mesothelioma [42-44], and further the investigation into BNCT and HVJ-E. However, some problems need to be resolved in future experiments, particularly with regard to improving the incorporation of $^{10}$B into the HVJ-E.

It has been reported that locally administered HVJ-E induces immuno-responses against tumors [23. 24], and effectively transports antitumor drugs [22,45]. Our experiments included a single administration of HVJ-E, which did not appear to have an anti-tumor effect unless accompanied by irradiation (Figure 5B, Additional file 2, Figure S2). However, the fractionated administration of HVJ-E, as is used for other vaccinations, might be possible. To address the limitations of this novel HVJ-E BSH, investigations into concurrent chemo-radiation therapy, fractionated administration with or without $^{10}$B, and conjugating with ligands for tumor-specific molecules should be performed.

In summary, we developed a form of CG-HVJ-E that could be administered into the general circulation and had both high tumor selectivity and high retention in tumor cells. This vector, when combined with BSH, improved the efficacy of BNCT for multiple liver tumors *in vivo*. Therefore, CG-HVJ-E holds potential for a drug delivery system with clinical applications for cancer therapy.

## Additional material

**Additional file 1: Figure S1. Transmission electron microscope photographs of HVJ-E complexes.** (A) HVJ-E, (B) CG-HVJ-E, and (C) CG-HVJ-E-BSH. Bar: 200 nm.

**Additional file 2: Figure S2. Survival of mice treated with BNCT.** Mice were given a single intra-cardiac injection of CG-HVJ-E-BSH (1.2 μg boron/g) 24 hours before irradiation, or BSH (1.3 μg boron/g) 1 hour before irradiation. PBS and CG-HVJ-E-BSH were administered without irradiation as a control. The mean survival time of the mice that received the BNCT treatment with CG-HVJ-E-BSH was significantly longer than that of the other groups (n = 4). * $p < 0.005$ (PBS without neutron irradiation, 1.3 μg boron/g of BSH with neutron irradiation, 1.2 μg boron/g of CG-HVJ-E-BSH without neutron irradiation vs. 1.2 μg boron/g of CG-HVJ-E-BSH with neutron irradiation).

**Additional file 3: Figure S3. Representative light microscopy views of the liver tumor (A) and normal liver tissue (B) 6 days after BNCT with a low dose of BSH (1.3 μg boron/g).** Tissues were stained with hematoxylin-eosin. Bar: 100 μm.

### Abbreviations

BNCT: Boron Neutron Capture Therapy; BSH: sodium borocaptate; HVJ-E: Hemagglutinating Virus of Japan Envelope.

### Acknowledgements

This work was supported in part by a grant for research and development of a Fixed Field Alternating Gradient Accelerator and DDS for BNCT from the New Energy and Industrial Technology Development Organization (NEDO), a Health Labour Science Research Grant from the Ministry of Health, Labour and Welfare of Japan, and a grant-in-Aid for Exploratory Research from the Ministry of Education, Culture, Sports, Science and Technology (MEXT).

### Author details

[1]Department of Surgery, Osaka University Graduate School of Medicine, Osaka, Japan. [2]Medical Center for Translational Research, Osaka University Hospital, Osaka, Japan. [3]Particle Radiation Oncology Research Center Laboratory, Research Reactor Institute, Kyoto University, Osaka, Japan. [4]Department of Agriculture, Osaka Prefectural University, Osaka, Japan. [5]Department of Biomaterials, Institute for Frontier Medical Sciences, Kyoto University, Kyoto, Japan. [6]Division of Gene Therapy Science, Osaka University Graduate School of Medicine, Osaka, Japan. [7]Health Care Economics and Industrial Policy, Osaka University Graduate School of Medicine, Osaka Japan.

### Authors' contributions

HF carried out the study, and contributed to the conception of the manuscript and the interpretations of the data. AM, HK, MS, MS, AT, and YT participated in the design of the study. YD, MK, and KO provided some intellectual recommendation. YK and YS provided some intellectual recommendation and reviewed the manuscript. CML conceived of the study, and participated in its design and coordination. All authors read and approved the final manuscript.

### Competing interests

All authors declare there were no actual or potential conflicts of interest in this study.

Received: 17 October 2010 Accepted: 20 January 2011
Published: 20 January 2011

### References

1. Barth RF, Coderre JA, Vicente MG, Blue TE: **Boron neutron capture therapy of cancer: current status and future prospects.** *Clin Cancer Res* 2005, **11**:3987-4002.
2. Yamamoto T, Nakai K, Matsumura A: **Boron neutron capture therapy for glioblastoma.** *Cancer Lett* 2008, **262**:143-52.
3. Pinelli T, Zonta A: **From the first idea to the application to the human liver.** Research and development in Neutron Capture Therapy; 2002.
4. Suzuki M, Sakurai Y, Hagiwara S, Masunaga S, Kinashi Y, Nagata K, Maruhashi A, Kudo M, Ono K: **First attempt of boron neutron capture therapy (BNCT) for hepatocellular carcinoma.** *Jpn J Clin Oncol* 2007, **37**:376-81.
5. Wittig A, Malago M, Collette L, Huiskamp R, Buhrmann S, Nievaart V, Kaiser G, Jockel KH, Sauerwein W: **BNCT in liver metastases: results of the EORTC trial 11001.** *Strahlentherapie Und Onkologie* 2007, **183**:115-115.
6. Sauerwein W, Malago M, Moss R, Altieri S, Hampel G, Wittig A, Nievaart V, Collette L, Mauri P, Huiskamp R, Michel J, Daquino G, Gerken G, Bornfeld N, Broelsch CE: **Boron Neutron Capture Therapy (BNCT) for the treatment of**

**diffuse, non-resectable liver metastases.** *Strahlentherapie Und Onkologie* 2006, **182**:109-109.

7. Cardose JE, Trivillin VA, Heber EM, Nigg DW, Calzetta O, Blaumann H, Longhino J, Itoiz ME, Bumaschny E, Pozzi E, Schwint AE: **Effect of Boron Neutron Capture Therapy (BNCT) on normal liver regeneration: Towards a novel therapy for liver metastases.** *International Journal of Radiation Biology* 2007, **83**:699-706.
8. Chou FI, Chung HP, Liu HM, Chi CW, Lui WY: **Suitability of boron carriers for BNCT: Accumulation of boron in malignant and normal liver cells after treatment with BPA, BSH and BA.** *Applied Radiation and Isotopes* 2009, **67**:S105-108.
9. Wittig A, Malago M, Collette L, Huiskamp R, Buhrmann S, Nievaart V, Kaiser GM, Jockel KH, Schmid KW, Ortmann U, Sauerwein WA: **Uptake of two $^{10}$B-compounds in liver metastases of colorectal adenocarcinoma for extracorporeal irradiation with boron neutron capture therapy (EORTC Trial 11001).** *Int J Cancer* 2008, **122**:1164-71.
10. Suzuki M, Masunaga SI, Kinashi Y, Takagaki M, Sakurai Y, Kobayashi T, Ono K: **The effects of boron neutron capture therapy on liver tumors and normal hepatocytes in mice.** *Jpn J Cancer Res* 2000, **91**:1058-64.
11. Sakurai Y, Ono K, Miyatake S, Maruhashi A: **Improvement effect on the depth-dose distribution by CSF drainage and air infusion of a tumour-removed cavity in boron neutron capture therapy for malignant brain tumours.** *Phys Med Biol* 2006, **51**:1173-83.
12. Wu G, Barth RF, Yang W, Lee RJ, Tjarks W, Backer MV, Backer JM: **Boron containing macromolecules and nanovehicles as delivery agents for neutron capture therapy.** *Anticancer Agents Med Chem* 2006, **6**:167-84.
13. Mehta SC, Lu DR: **Targeted drug delivery for boron neutron capture therapy.** *Pharm Res* 1996, **13**:344-51.
14. Maruyama K, Ishida O, Kasaoka S, Takizawa T, Utoguchi N, Shinohara A, Chiba M, Kobayashi H, Eriguchi M, Yanagie H: **Intracellular targeting of sodium mercaptoundecahydrododecaborate (BSH) to solid tumors by transferrin-PEG liposomes, for boron neutron-capture therapy (BNCT).** *J Control Release* 2004, **98**:195-207.
15. Masunaga S, Kasaoka S, Maruyama K, Nigg D, Sakurai Y, Nagata K, Suzuki M, Kinashi Y, Maruhashi A, Ono K: **The potential of transferrin-pendant-type polyethyleneglycol liposomes encapsulating decahydrodecaborate-($^{10}$B) (GB-10) as $^{10}$B-carriers for boron neutron capture therapy.** *Int J Radiat Oncol Biol Phys* 2006, **66**:1515-22.
16. Doi A, Kawabata S, Iida K, Yokoyama K, Kajimoto Y, Kuroiwa T, Shirakawa T, Ishikawa M, Kasaoka S, Maruyama K, Kumada H, Sakurai Y, Masunaga S, Ono K, Miyatake S: **Tumor-specific targeting of sodium borocaptate (BSH) to malignant glioma by transferrin-PEG liposomes: a modality for boron neutron capture therapy.** *J Neurooncol* 2008, **87**:287-94.
17. Aljabiri MR, Lodato F, Burroughs AK: **Surveillance and diagnosis for hepatocellular carcinoma.** *Liver Transpl* 2007, **13(11 Suppl 2)**:S2-12.
18. World Health Organization: **World Health Statistics 2008/Future trends in global mortality.**[http://www.who.int/whosis/whostat/2008/en/index.html].
19. Arciero CA, Sigurdson ER: **Diagnosis and treatment of metastatic disease to the liver.** *Semin Oncol* 2008, **35**:147-59.
20. Kaneda Y, Nakajima T, Nishikawa T, Yamamoto S, Ikegami H, Suzuki N, Nakamura H, Morishita R, Kotani H: **Hemagglutinating virus of Japan (HVJ) envelope vector as a versatile gene delivery system.** *Mol Ther* 2002, **6**:219-26.
21. Mima H, Yamamoto S, Ito M, Tomoshige R, Tabata Y, Tamai K, Kaneda Y: **Targeted chemotherapy against intraperitoneally disseminated colon carcinoma using a cationized gelatin-conjugated HVJ envelope vector.** *Mol Cancer Ther* 2006, **5**:1021-8.
22. Kawano H, Komaba S, Kanamori T, Kaneda Y: **A new therapy for highly effective tumor eradication using HVJ-E combined with chemotherapy.** *BMC Med* 2007, **5**:1-7.
23. Kurooka M, Kaneda Y: **Inactivated Sendai virus particles eradicate tumors by inducing immune responses through blocking regulatory T cells.** *Cancer Res* 2007, **67**:227-36.
24. Fujihara A, Kurooka M, Miki T, Kaneda Y: **Intratumoral injection of inactivated Sendai virus particles elicits strong antitumor activity by enhancing local CXCL10 expression and systemic NK cell activation.** *Cancer Immunol Immunother* 2008, **57**:73-84.
25. Mima H, Tomoshige R, Kanamori T, Tabata Y, Yamamoto S, Ito S, Tamai K, Kaneda Y: **Biocompatible polymer enhances the in vitro and in vivo transfection efficiency of HVJ envelope vector.** *J Gene Med* 2005, **7**:888-97.
26. Asai T, Ueda T, Itoh K, Yoshioka K, Aoki Y, Mori S, Yoshikawa H: **Establishment and characterization of a murine osteosarcoma cell line (LM8) with high metastatic potential to the lung.** *Int J Cancer* 1998, **76**:418-422.
27. Lee CM, Tanaka T, Murai T, Kondo M, Kimura J, Su W, Kitagawa T, Ito T, Matsuda H, Miyasaka M: **Novel chondroitin sulfate-binding cationic liposomes loaded with cisplatin efficiently suppress the local growth and liver metastasis of tumor cells in vivo.** *Cancer Res* 2002, **62**:4282-8.
28. Fukunaka Y, Iwanaga K, Morimoto K, Kakemi M, Tabata Y: **Controlled release of plasmid DNA from cationized gelatin hydrogels based on hydrogel degradation.** *J Control Release* 2002, **80**:333-43.
29. Hosseinkhani H, Aoyama T, Ogawa O, Tabata Y: **Ultrasound enhancement of in vitro transfection of plasmid DNA by a cationized gelatin.** *J Drug Target* 2002, **10**:193-204.
30. Nagata I, Kimura Y, Ito Y, Tanaka T: **Temperature-Sensitive Phenomenon of Viral Maturation Observed in BHK Cells Persistently Infected with HVJ.** *Virology* 1972, **49**:453-461.
31. Guttenberger M: **Protein Determination.** *Cell Biology* A Laboratory Handbook:295-303.
32. Ogura K, Yanagie H, Eriguchi M, Lehmann EH, Kuhne G, Bayon G, Kobayashi H: **Neutron capture autoradiographic study of the biodistribution of $^{10}$B in tumor-bearing mice.** *Appl Radiat Isot* 2004, **61**:585-90.
33. Saga K, Tamai K, Kawachi M, Shimbo T, Fujita H, Yamazaki T, Kaneda Y: **Functional modification of Sendai virus by siRNA.** *J Biotechnol* 2008, **133**:386-94.
34. Maeda H, Wu J, Sawa T, Matsumura Y, Hori K: **Tumor vascular permeability and the EPR effect in macromolecular therapeutics: a review.** *J Control Release* 2000, **65**:271-84.
35. Siwak DR, Tari AM, Lopez-Berestein G: **The potential of drug-carrying immunoliposomes as anticancer agents. Commentary re: J. W. Park et al., Anti-HER2 immunoliposomes: enhanced efficacy due to targeted delivery.** *Clin Cancer Res* 2002, **8**:1172-1181, Clin Cancer Res 2002;8:955-6.
36. Yanagie H: **Selective Enhancement of Boron Accumulation with Boron-Entrapped Water-in-oil-in-water Emulsion in VX-2 Rabbit Hepatic Cancer Model for BNCT.** Proc of 12th International Congress of Neutron Capture Therapy; 2006.
37. Ye SJ: **Monte Carlo based protocol for cell survival and tumour control probability in BNCT.** *Phys Med Biol* 1999, **44**:447-61.
38. Kobayashi T, Kanda K: **Analytical calculation of boron- 10 dosage in cell nucleus for neutron capture therapy.** *Radiat Res* 1982, **91**:77-94.
39. Kinashi Y, Masunaga S, Nagata K, Suzuki M, S T, Ono K: **A bystander effect observed in boron neutron capture therapy: A study of the induction of mutations in the HPRT locus.** *Int J Radiat Oncol Biol Phys* 2007, **68**:508-14.
40. Suzuki M, Sakurai Y, Masunaga S, Kinashi Y, Nagata K, Ono K: **Dosimetric study of boron neutron capture therapy with borocaptate sodium (BSH)/lipiodol emulsion (BSH/lipiodol-BNCT) for treatment of multiple liver tumors.** *Int J Radiat Oncol Biol Phys* 2004, **58**:892-6.
41. Suzuki M, Nagata K, Masunaga S, Kinashi Y, Sakurai Y, Maruhashi A, Ono K: **Biodistribution of $^{10}$B in a rat liver tumor model following intra-arterial administration of sodium borocaptate (BSH)/degradable starch microspheres (DSM) emulsion.** *Appl Radiat Isot* 2004, **61**:933-7.
42. Yanagie H, Tonita T, Kobayashi H, Fujii Y, Nonaka Y, Saegusa Y, Hasumi K, Eriguchi M, Kobayashi T, Ono K: **Inhibition of human pancreatic cancer growth in nude mice by boron neutron capture therapy.** *Br J Cancer* 1997, **75**:660-5.
43. Yanagie H, Sakurai Y, Ogura K, Kobayashi T, Furuya Y, Sugiyama H, Kobayashi H, Ono K, Nakagawa K, Takahashi H, Nakazawa M, Eriguchi M: **Evaluation of neutron dosimetry on pancreatic cancer phantom model for application of intraoperative boron neutron-capture therapy.** *Biomed Pharmacother* 2007, **61**:505-14.
44. Suzuki M, Sakurai Y, Masunaga S, Kinashi Y, Nagata K, Maruhashi A, Ono K: **A preliminary experimental study of boron neutron capture therapy for malignant tumors spreading in thoracic cavity.** *Jpn J Clin Oncol* 2007, **37**:245-9.
45. Kawano H, Komaba S, Yamasaki T, Maeda M, Kimura Y, Maeda A, Kaneda Y: **New potential therapy for orthotopic bladder carcinoma by combining HVJ envelope with doxorubicin.** *Cancer Chemother Pharmacol* 2008, **61**:973-8.

doi:10.1186/1748-717X-6-8
**Cite this article as:** Fujii *et al.*: Cationized gelatin-HVJ envelope with sodium borocaptate improved the BNCT efficacy for liver tumors *in vivo*. *Radiation Oncology* 2011 **6**:8.

TISSUE ENGINEERING: Part C
Volume 17, Number 2, 2011

DOI: 10.1089/ten.tec.2010.0139

# Transplantation of Human Adipose Tissue-Derived Multilineage Progenitor Cells Reduces Serum Cholesterol in Hyperlipidemic Watanabe Rabbits

Hanayuki Okura, Ph.D.,[1,2] Ayami Saga, M.S.,[1] Yuichi Fumimoto, M.D., Ph.D.,[1] Mayumi Soeda, V.M.D.,[1] Mariko Moriyama, Ph.D.,[1,3] Hiroyuki Moriyama, Ph.D.,[3] Koji Nagai, M.D.,[1,4] Chun-Man Lee, M.D., Ph.D.,[1] Shizuya Yamashita, M.D., Ph.D.,[5] Akihiro Ichinose, M.D., Ph.D.,[4] Takao Hayakawa, Ph.D.,[3] and Akifumi Matsuyama, M.D., Ph.D.[1]

Familial hypercholesterolemia (FH) is an autosomal codominant disease characterized by high concentrations of proatherogenic lipoproteins and premature atherosclerosis secondary to low-density lipoprotein (LDL) receptor deficiency. We examined a novel cell therapy strategy for the treatment of FH in the Watanabe heritable hyperlipidemic (WHHL) rabbit, an animal model for homozygous FH. We delivered human adipose tissue-derived multilineage progenitor cells (hADMPCs) via portal vein and followed by immunosuppressive regimen to avoid xenogenic rejection. Transplantation of hADMPCs resulted in significant reductions in total cholesterol, and the reductions were observed within 4 weeks and maintained for 12 weeks. $^{125}$I-LDL turnover study showed that the rate of LDL clearance was significantly higher in the WHHL rabbits with transplanted hADMPCs than those without transplanted. After transplantation hADMPCs were localized in the portal triad, subsequently integrated into the hepatic parenchyma. The integrated cells expressed human albumin, human alpha-1-antitrypsin, human Factor IX, human LDL receptors, and human bile salt export pump, indicating that the transplanted hADMPCs resided, survived, and showed hepatocytic differentiation *in vivo* and lowered serum cholesterol in the WHHL rabbits. These results suggested that hADMPC transplantation could correct the metabolic defects and be a novel therapy for inherited liver diseases.

## Introduction

Familial hypercholesterolemia (FH) is characterized by premature and accelerated development of atherosclerotic lesions caused by elevated levels of cholesterol-rich lipoproteins in plasma. The disease is caused by mutations in the low-density lipoprotein (LDL) receptor gene that result in a significant decrease in receptor-mediated uptake of lipoproteins from the circulation.[1–3] Patients homozygous for defects in LDL receptors have serum cholesterol levels 5–10 times those of normal and suffer as early as the first two decades of life from complications such as coronary artery disease.[4,5] In homozygous FH patients, conventional drug therapy cannot treat the condition, and therapeutic recourses are limited to chronic plasmapheresis or orthotopic liver transplantation.[1] Although liver transplants lower LDL levels, the procedure is life threatening; in addition, donor livers are in short supply. Cellular transplantation has been proposed to provide functional LDL receptors for the treatment of hypercholesterolemia. Transplantation of allogenic and xenogenic hepatocytes has been shown to be effective in lowering serum cholesterol in the Watanabe heritable hyperlipidemic (WHHL) rabbit,[6–9] which is an animal model for homozygous FH. Further, a number of gene therapy approaches have shown some promises in animal models and human,[10–13] and the therapies will cure a number of patients with FH in near future. As an alternative to whole-organ transplantation and/or gene therapy, we have investigated the ability of human adipose tissue-derived multilineage progenitor cells (hADMPCs) to differentiate into hepatocytes *in vitro* and to replace critical liver functions[14] as well as previous reports,[15,16] because the *in vitro* differentiation of hADMPCs into various kinds of cell types in now well reported and hADMPCs can be easily and safely obtained in large

[1]Department of Somatic Stem Cell Therapy and Health Policy, Foundation for Biomedical Research and Innovation, Kobe, Japan.
[2]Research Fellow of the Japan Society for the Promotion of Science, Tokyo, Japan.
[3]Pharmaceutical Research and Technology Institute, Kinki University, Osaka, Japan.
[4]Department of Plastic Surgery, Kobe University Hospital, Kobe, Japan.
[5]Division of Cardiology, Department of Internal Medicine, Osaka University Graduate School of Medicine, Osaka Japan.

quantities without serious ethics issues.[17,18] In this study, we are investigating whether hADMPCs could differentiate into hepatocytes *in vivo* and replace critical liver functions as considerable therapeutic potential for cellular replacement.

## Materials and Methods

### *Cells*

hADMPCs were prepared as described previously[19] with some modifications.[14,17,18] Adipose tissues from human subjects were resected during plastic surgery in five subjects (four males and one female, age, 20–60 years) as excess discards. Ten to 50 g of subcutaneous adipose tissue was collected from each subject. All subjects provided informed consent. The protocol was approved by the Review Board for Human Research of Kobe University Graduate School of Medicine, Osaka University Graduate School of Medicine, and Foundation for Biomedical Research and Innovation. After five to six passages, the hADMPCs were used for transplantation. Human cryopreserved hepatocytes were purchased from Invitrogen (Lot number: HuP81) and cultured as indicated by the manufacturer's protocol. Human adipose tissue-derived fibroblastic cells were obtained according to previous report.[20]

### *Flow cytometric analysis*

hADMPCs isolated from adipose tissue were characterized by flow cytometry. Cells were detached from culture dishes by 0.25% trypsin/ethylenediaminetetraacetic acid (EDTA) and suspended in Dulbecco's phosphate-buffered saline (DPBS; Nacalai Tesque) containing 0.1% fetal bovine serum. Aliquots ($5\times10^5$ cells) were incubated for 30 min at 4°C with fluorescein isothiocyanate-conjugated mouse monoclonal antibodies to human CD31 (BD PharMingen), CD105 (Ancell Corporation), CD133 (R&D Systems), phycoerythrin-conjugated mouse monoclonal antibodies to human CD29, CD34, CD45, CD73 (BD PharMingen), CD44, or CD166 (Ancell). Isotype-identical antibodies served as controls. Further, the cells were incubated with mouse monoclonal antibodies against human stage-specific embryonic antigen-4 (from Chemicon International, Inc.), ABCG-2, or CD117 (BD PharMingen) with nonspecific mouse antibody used as a negative control. After washing with DPBS, cells were incubated with phycoerythrin-labeled goat anti-mouse Ig antibody (BD PharMingen) for 30 min at 4°C. After three washes, cells were resuspended in DPBS and analyzed by flow cytometry using a FACSCalibur flow cytometer and CellQuest Pro software (BD Biosciences).

### *Adipogenic, osteogenic, and chondrogenic differentiation procedure*

For adipogenic differentiation, cells were cultured in the differentiation medium (Zen-Bio, Inc.). After 3 days, half of the medium was changed with adipocyte medium (Zen-Bio) every 2 days. Five days after differentiation, adipocytes were characterized by microscopic observation of intracellular lipid droplets by Oil Red O staining. Osteogenic differentiation was induced by culturing the cells in Dulbecco's modified Eagle's medium containing 10 nM dexamethasone, 50 mg/dL ascorbic acid 2-phosphate, 10 mM β-glycerophosphate (Sigma), and 10% fetal bovine serum. Differentiation was examined by Alizarin red staining. For Alizarin red staining, the cells were washed three times and fixed with dehydrated ethanol. After fixation, the cells were stained with 1% Alizarin red S in 0.1% $NH_4OH$ (pH 6.5) for 5 min and then washed with $H_2O$. For chondrogenic differentiation, hADMPCs were first trypsinized and $2\times10^5$ cells were centrifuged at 400 *g* for 10 min. The resulting pellets were cultured in the chondrogenic medium (alpha-minimum essential medium (alpha-MEM) supplemented with 10 ng/mL transforming growth factor-β, 10 nM dexamethasone, 100 μM ascorbate, and 10 μL/mL 100×ITS Solution) for 14 days. For Alcian Blue staining, nuclear counterstaining with Weigert's hematoxylin was followed by 0.5% Alcian Blue 8GX for proteoglycan-rich cartilage matrix.

### *hADMPC transplantation and immunosuppression regimen*

WHHL rabbits (8 weeks old; purchased from Kitayamalabes, Inc.) were anesthetized with pentobarbital (50 mg/kg). An incision distal and parallel to the lower end of the ribcage was made. The peritoneum was incised, and hADMPCs ($n=5$) or human adipose tissue-derived fibroblastic cells ($n=3$) ($3\times10^7$ cells) suspended in 3 mL of Hanks' balanced salt solutions (HBSS) (20°C) or 3 mL of control saline ($n=6$) were infused in 5 min into the portal vein via a 18-gauge Angiocath™ (BD). The immunosuppression regimen (Fig. 1A) consisted of the following: (1) intramuscular injection of cyclosporin A (6 mg/kg/day) daily from the day before surgery to sacrifice; (2) intramuscular injection of rapamycin (0.05 mg/kg/day) daily from the day before surgery to sacrifice; (3) methylprednisolone at 3 mg/kg/day (days 1–7), followed by tapering to 2 mg/kg/day (days 8–14), 1 mg/kg/day (days 15–21) and 0.5 mg/kg/day (day 22 to the time at sacrifice); (4) intravenous injection of cyclophosphamide (20 mg/kg/day) at days 0, 2, 5, and 7; (5) ganciclovir (2.5 mg/kg/day intramuscular injection (i.m.)) was also administrated to avoid viral infection in the immunocompromised host.

### *DNA extraction and quantification of human-derived cells*

Total DNA of WHHL rabbit liver, which was obtained at the time just after hADMPC transplantation, and 2, 4, 8, and 12 weeks after transplantation, were isolated using a NucleoSpin Tissue kit (Macherey-Nagel) according to the manufacturer's instructions. hADMPCs and rabbit hepatocytes were mixed at the ratios of 100:0 (100%), 10:90 (10%), 1:99 (1%), 0.1:99.9 (0.1%), 0.01:99.99 (0.01%), and 0.001:99.999 (0.001%), and DNA was isolated. Seven hundred nanograms of each samples of extracted DNA was quantified by real-time polymerase chain reaction (PCR) using the ABI Prism 7900 Sequence Detection System (Applied Biosystems), primers for the 82 bp *Alu* amplicon (forward, 5′-GTCAGGAGATCGA GACCATCCC; reverse, 5′-CCACTACGCCCGGCTAATTT), and SYBR Green (TOYOBO) dye using a previously published protocol.[21,22] Reactions were performed in quadruplicate and the *Alu* levels were calculated by the standard curve.

### *Assay for lipid profiling*

Serum samples were obtained from nonfasting rabbits before and after transplantation. Serum total cholesterol was measured in each sample using assay kits from Wako Pure Chemical Industries. Serum lipoproteins were analyzed by an on-line dual enzymatic method for simultaneous quantification of cholesterol and triglycerides by high-performance

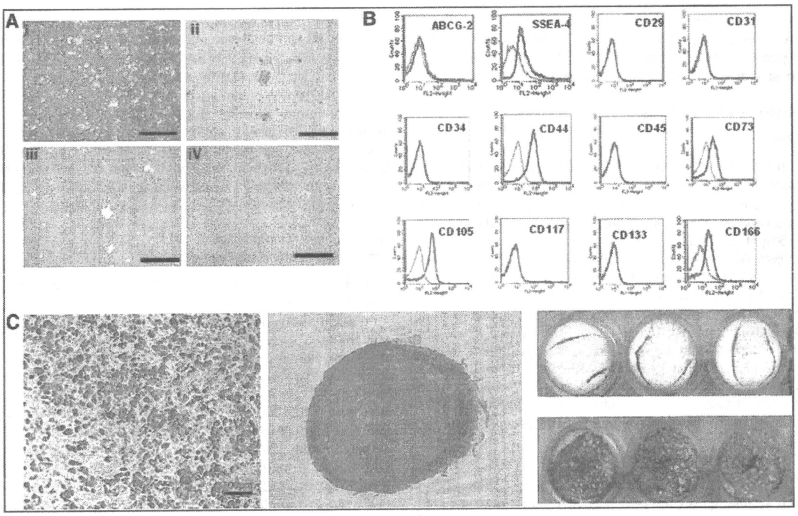


FIG. 1. **(A)** Morphological characters of human adipose tissue-derived multilineage progenitor cells (hADMPCs). The cells obtained from adipose tissue were seeded and incubated for 24 h **(i)**. After incubation, the adherent cells were treated with ethylenediaminetetraacetic acid solution, and the resulting suspended cells were replated at a density of 10,000 cells/cm$^2$ on human fibronectin-coated dishes (BD BioCoat) **(ii, iii)**. Within two to three passages after the initial plating of the primary culture, hADMPCs appeared as a monolayer of large flat cells (25–30 μm in diameter). As the cells approached confluence, they assumed a more spindle-shaped, fibroblastic morphology **(iv)**. i) Bar = 499 μm, ii) bar = 201 μm, iii) bar = 502 μm and iv) bar = 202 μm. **(B)** Cell surface markers expressed on hADMPCs. The cells were negative for markers of the hematopoietic lineage (CD45) and of hematopoietic stem cells, ABCG-2, CD34, and CD133. They were also negative for CD31, an endothelial cell-associated marker, and the surface antigen c-Kit (CD117). However, they stained positively for a number of surface markers characteristic of mesenchymal and/or neural stem cells, but not embryonic stem (ES) cells, including CD29, CD44 (hyaluronan receptor), CD73, CD105 (endoglin), and CD166. hADMPCs also were positive for stage-specific embryonic antigen (SSEA)-4. **(C)** Adipocytic, chondrocytic, and osteocytic differentiation potentials of hADMPCs. Adipocytic differentiation potential of hADMPCs was confirmed by Oil Red O staining (the left panel) (bar = 100 μm). Chondrocytic differentiation potential of hADMPCs was estimated by extracellular matrices with Alcian Blue staining (the middle panel). Osteogenic differentiation potential of hADMPCs was confirmed by Alizarin red S staining for mineralized nodules (the right panel).

liquid chromatography at Skylight Biotech, according to the procedure as described.[23]

### *Immunohistochemical staining of WHHL rabbit liver sections*

The WHHL livers were harvested and fixed immediately with 10% formalin. They were placed into optimal cutting temperature compound (Sakura Finetechnical Co.), frozen immediately, and then sectioned at 7 μm thickness. The sections were then incubated with blocking solution (Blocking one; Nacalai Tesque) for 1 h. The samples were incubated with rabbit anti-human-specific albumin antibody (MBL), rabbit anti-human-specific alpha 1 anti-trypsin antibody, and rabbit anti-LDL receptor antibody, followed by Alexa Fluor 488-labeled goat anti-rabbit IgG (Molecular Probes). To show the colocalization of human CD90 and albumin, the samples were incubated with the rabbit anti-human CD90 monoclonal antibody (Epitomics, Inc.) and then with Alexa Fluor 488-labeled goat anti-rabbit IgG (Molecular Probes), and washed extensively. Then, the specimens were incubated with rabbit anti-human-specific albumin antibody (MBL), followed by Alexa Fluor 546-labeled goat anti-rabbit IgG (Molecular Probes). The treated sample was examined with a BioZero laser scanning microscope (Keyence).

### *PCR analysis of WHHL rabbit liver for human liver-specific genes*

Total RNAs of WHHL rabbit liver, hADMPCs, and human hepatocytes were isolated using an RNAeasy kit (Qiagen). After treatment with DNase, the cDNA was synthesized using Superscript III RNase H-minus Reverse Transcriptase (Invitrogen). Real-time PCR was performed using the ABI Prism 7900 Sequence Detection System (Applied Biosystems). About 20× Assays-on-Demand™ Gene Expression Assay Mix for human alpha-1-antitrypsin (Hs01097800_m1), human albumin (Hs00609411_m1), human factor 9, human GATA-binding

protein 4 (GATA4) (Hs00171403_m1), human hepatocyte nuclear factor 3 beta (Hs00232764_m1), human LDL receptor (Hs00181192_m1), and human glyceraldehyde-3-phosphate dehydrogenase (Hs99999905_m1) were obtained from Applied Biosystems. It was confirmed that human detectors and rabbit detectors do not cross-react with the other species. TaqMan® Universal PCR Master Mix, No AmpErase® UNG (2×), was also purchased from Applied Biosystems. Reactions were performed in quadruplicate and the mRNA levels were normalized relative to human glyceraldehyde-3-phosphate dehy-

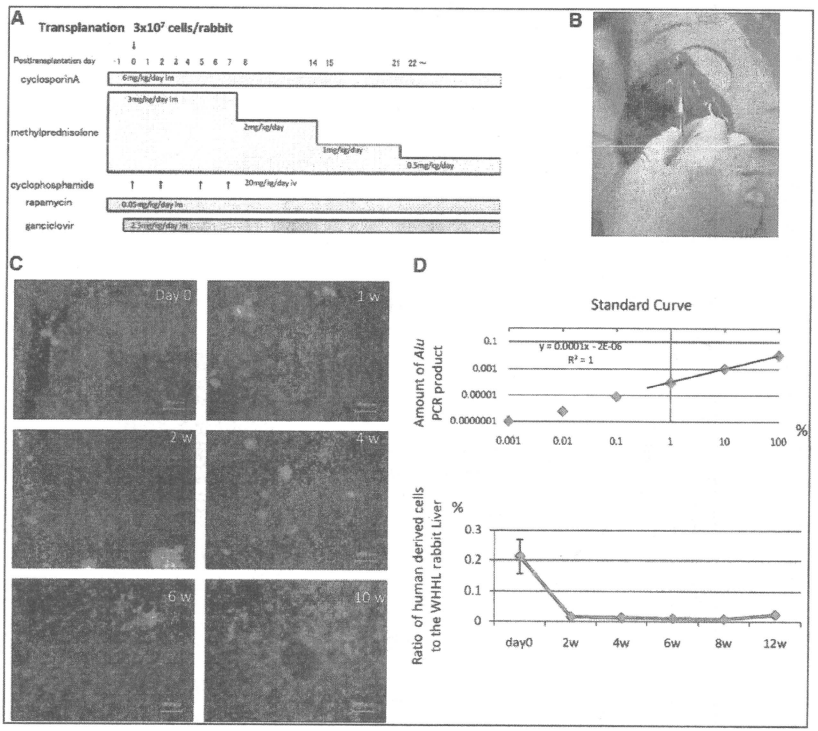


FIG. 2. **(A)** Immunosuppression regimen. Cyclosporin A (6 mg/kg/day) and rapamycin (0.05 mg/kg/day) were administered intramuscularly daily from the day before surgery to sacrifice. Methylprednisolone was administered at 3 mg/kg/day (days 1–7), 2 mg/kg/day (days 8–14), 1 mg/kg/day (days 15–21), and 0.5 mg/kg/day (day 22 to sacrifice). Cyclophosphamide (20 mg/kg/day) was injected intravenously at days 0, 2, 5, and 7. Ganciclovir (2.5 mg/kg/day) was also injected intramuscularly to avoid viral infection in the immunocompromised host. **(B)** Surgical procedure. Watanabe heritable hyperlipidemic (WHHL) rabbits were anesthetized with pentobarbital. An incision was made distal and parallel to the lower end of the ribcage. The peritoneum was incised and hADMPCs, and human adipose tissue-derived fibroblastic cells (hADFCs) ($3\times10^7$ cells/rabbit) or controls were infused into the portal vein using an 18-gauge Angiocath. **(C)** Localization of transplanted hADMPCs in the WHHL liver. At the day of and 1, 2, 4, 6, and 10 weeks after transplantation of DiI-labeled hADMPCs via the portal vein, the WHHL rabbit liver was examined histologically. DiI-fluorescent labeled-hADMPCs resided and distributed in the portal area at the day of transplantation. One to 2 weeks after transplantation, the DiI-stained hADMPCs-derived cells were localized near the portal areas. Four weeks after transplantation some of the DiI-stained cells resembled innate hepatocytes morphologically. Six and 10 weeks after transplantation, DiI-positive transplanted cells were dispersed in a centrilobular direction, resembling the mature innate hepatocytes. Bars = 100 μm. **(D)** Quantification of repopulation of the transplanted cells in the liver. The ratios of human-derived cell repopulation were examined by analyzing an *Alu* repetitive DNA sequence at the day of and 2, 4, 8, and 12 weeks after transplantation. In upper panel the standard curve was indicated, and in lower panel the ratio of repopulation of human cells was shown in time course after transplantation of hADMPCs.

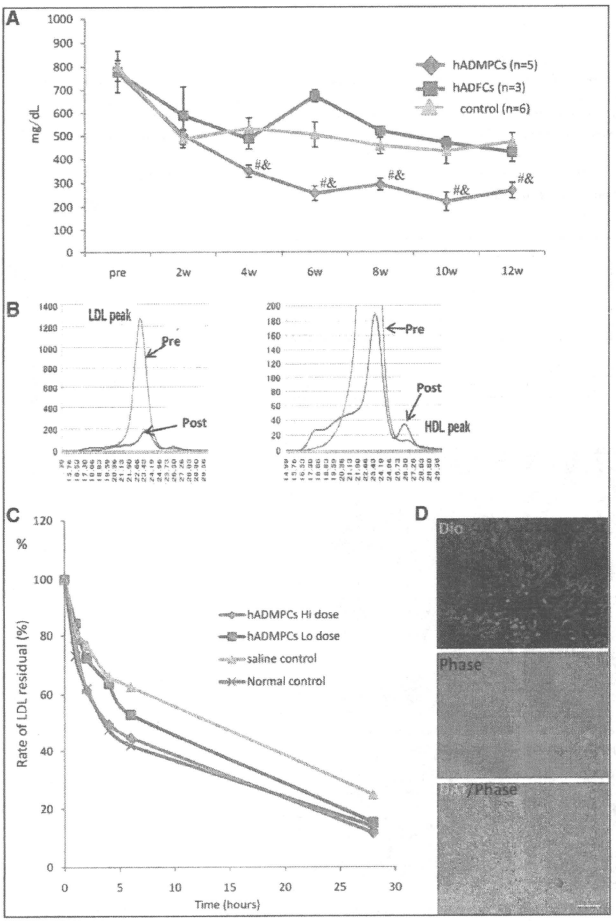


FIG. 3. **(A)** Total serum cholesterol levels. hADMPC transplantation in WHHL rabbits was followed for 12 weeks. Total serum cholesterol was measured in five rabbits that each received $3\times10^7$ hADMPCs, three rabbits that each received $3\times10^7$ hADFCs, and in six rabbits that received saline (control). Bars indicated mean ± standard error of the mean (SEM) ($^{\#}p < 0.05$; control vs. the hADMPC-transplanted WHHL rabbit; $^{\&}p < 0.05$; the hADFC-transplanted WHHL rabbit vs. the hADMPC-transplanted WHHL rabbit). **(B)** Lipoprotein profiles in a representative WHHL rabbit with hADMPC transplantation after gel filtration. Serum samples from the WHHL rabbit before and 4 weeks after transplantation were fractionated. Note the marked reduction in low-density lipoprotein (LDL) peak and appearance of high-density lipoprotein (HDL) peak. **(C)** Rate of clearance of LDL from the serum of rabbits with and without transplantation of hADMPCs. Animals were injected with $^{125}$I-labeled human LDL, and the time course of clearance was monitored following trichroloacetic acid precipitation of serum at time 5 min, 1 h, 2 h, 4 h, 6 h, and 28 h. Residual $^{125}$I-LDL was expressed as percentages of that at 5 min. $^{*}p < 0.05$ (control vs. the hADMPC-transplanted WHHL rabbit [low dose]) and $^{*}p < 0.05$ (control vs. the hADMPC-transplanted WHHL rabbit [high dose]). **(D)** DiO-LDL uptake into hADMPC-derived hepatocytes in the WHHL rabbi liver. Thin-sliced recipient liver was incubated with DiO-labeled LDL in the serum-free medium for 24 h. After washing and fixation, the incubated slices were applied for fluorescent microscopy. DiO-LDL uptake cells (green) and no uptake parenchymal cells were observed in the section. Bar = 100 μm.

drogenase expression. To confirm that hADMPCs differentiated into hepatocytes *in vivo*, the cells before transplantation and human primary hepatocytes (Invitrogen, Lot number; HuP81) were applied for quantitative PCR as control.

### *Clearance of $^{125}$I-LDL from rabbit serum*

WHHL rabbits (8 weeks old) were anesthetized with pentobarbital (50 mg/kg). The peritoneum was incised and hADMPCs (high-dose; $3\times10^7$ cells/rabbit, $n=2$, low-dose; $5\times10^6$ cells/rabbit, $n=2$) suspended in 3 mL of HBSS (20°C) ($n=5$) or 3 mL of control saline ($n=2$) were infused into the portal vein via a 18-gauge Angiocath (BD). The rabbits were immunosuppressed using the protocol illustrated in Figure 1A. Eight weeks later, the animals were tested by the LDL turnover assay. $^{125}$I human LDL (BT-913R, Lot No. 9130709; Biomedical Technologies Inc.) was delivered via the marginal ear vein of the WHHL rabbits and normal control